



1 **Automated compound speciation, cluster analysis, and**
2 **quantification of organic vapours and aerosols using**
3 **comprehensive two-dimensional gas chromatography and**
4 **mass spectrometry**

5 Xiao He¹, Xuan Zheng^{1*}, Shuwen Guo¹, Lewei Zeng¹, Ting Chen¹, Bohan Yang¹,
6 Shupeixiao¹, Qiongqiong Wang², Zhiyuan Li³, Yan You⁴, Shaojun Zhang^{5,6,7,8}, and Ye
7 Wu^{5,6,7,8}

8 ¹College of Chemistry and Environmental Engineering, Shenzhen University, Shenzhen 518060, China

9 ²Department of Atmospheric Science, School of Environmental Studies, China University of
10 Geosciences, Wuhan 430074, China

11 ³School of Public Health (Shenzhen), Sun Yat-sen University, Guangzhou 510275, China

12 ⁴National Observation and Research Station of Coastal Ecological Environments in Macao, Macao
13 Environmental Research Institute, Macao University of Science and Technology, Macao SAR 999078,
14 China

15 ⁵School of Environment, State Key Joint Laboratory of Environment Simulation and Pollution Control,
16 Tsinghua University, Beijing 100084, China

17 ⁶State Environmental Protection Key Laboratory of Sources and Control of Air Pollution Complex,
18 Beijing 100084, China

19 ⁷Beijing Laboratory of Environmental Frontier Technologies, School of Environment, Tsinghua
20 University, Beijing 100084, China

21 ⁸Laboratory of Transport Pollution Control and Monitoring Technology, Transport Planning and
22 Research Institute, Ministry of Transport, Beijing 100028, China

23 *Correspondence to:* Xuan Zheng (x-zheng11@szu.edu.cn)



24 **Abstract:** The advancement of analytical techniques, such as comprehensive two-dimensional gas
25 chromatography coupled with mass spectrometry (GC×GC-MS), enables the efficient separation of
26 complex organic matrix. Developing innovative methods for data processing and analysis is crucial to
27 unlock the full potential of GC×GC-MS in understanding intricate chemical mixtures. In this study, we
28 proposed an innovative method for the semi-automated identification and quantification of complex
29 organic mixtures using GC×GC-MS. The method was formulated based on self-constructed mass
30 spectrum patterns and the traversal algorithms and was applied to organic vapor and aerosol samples
31 collected from tailpipe emissions of heavy-duty diesel vehicles and the ambient atmosphere. Thousands
32 of compounds were filtered, speciated, and clustered into 26 categories, including aliphatic and cyclic
33 hydrocarbons, aromatic hydrocarbons, aliphatic oxygenated species, phenols and alkyl-phenols, and
34 heteroatom containing species. The identified species accounted for over 80% of all the eluted
35 chromatographic peaks at the molecular level. A comprehensive analysis of quantification uncertainty
36 was undertaken. Using representative compounds, quantification uncertainties were found to be less than
37 37.67%, 22.54%, and 12.74% for alkanes, polycyclic aromatic hydrocarbons (PAHs), and alkyl-
38 substituted benzenes, respectively, across the GC×GC space, excluding the first and the last time
39 intervals. From source apportionment perspective, adamantane was clearly isolated as a potential tracer
40 for heavy-duty diesel vehicles (HDDVs) emission. The systematic distribution of N-containing
41 compounds in oxidized and reduced valences was discussed and many of them served as critical tracers
42 for secondary nitrate formation processes. The results highlighted the benefits of developing self-
43 constructed model for the enhanced peak identification, automated cluster analysis, robust uncertainty
44 estimation, and source apportionment and achieving the full potential of GC×GC-MS in atmospheric
45 chemistry.



46 **1 Introduction**

47 Improved sampling strategies, coupled with innovative measurement techniques, are imperative to
48 capture the dynamic nature of atmospheric chemistry, particularly in the context of climate change and
49 health risk (Franklin et al. 2023, Franklin et al. 2022, Huo et al. 2021, Phillips et al. 2018).
50 Comprehensive two-dimensional gas chromatography coupled with mass spectrometry (GC×GC-MS)
51 has emerged as a powerful tool for compound detection and identification, benefitting from the
52 combination of two columns with orthogonal selectivity (Alam et al. 2013, Franklin et al. 2022).
53 Despite its capabilities, GC×GC-MS encounters formidable challenges in data analysis, which can be
54 extremely complicated and demanding. Efforts have been made to delve into the deluge of data generated
55 by GC×GC-MS. Traditionally, mass spectra were deconvoluted and compared to spectra from the
56 National Institute of Standards and Technology (NIST20) library for peak identification with pre-defined
57 criteria (Guo et al. 2016, Piotrowski et al. 2018). Retention indices (RI) were further introduced to
58 distinguish homologous compounds with resembling mass spectra (Zang et al. 2023). A pioneering and
59 instructive work for searching criteria to classify GC×GC peaks was published in 2003 (Welthagen,
60 Schnelle-Kreis and Zimmermann 2003). Welthagen (2003) incorporated the mass fragmentation patterns
61 to classify compounds in atmospheric aerosol samples. Compounds belonging to the same chemical
62 group related to one another in the GC×GC space and distributed in a structured pattern. They
63 successfully identified seven groups of compounds, including alkanes, alkenes and cycloalkanes, alkyl
64 substituted benzenes, alkyl substituted polar benzenes, hydrated naphthalenes and alkenyl benzenes,
65 alkylated naphthalenes, and alkane acids, occupying more than 60% of the total peak area. This work set
66 a good example of how user-defined rule could facilitate the identification of specific compound groups.
67 Recent advances in chemometric tools for GC×GC-MS analysis involving machine learning and deep
68 learning renovate multi-dimensional chromatography fields (Stefanuto, Smolinska and Focant 2021).
69 Bendik (2021) developed a programming suite for high-confidence and fast compound identification
70 using GC×GC coupled with time-of-flight mass spectrometry (TOF-MS) (Bendik et al. 2021). He (2022)
71 extracted featured mass spectrometric information of the intermediate-volatility and semi-volatile
72 organic compounds (I/SVOCs) by integrating algorithmic language into GC×GC-MS data (He et al.
73 2022a, He et al. 2022b). A novel pixel-based multiway principal component analysis method was utilized
74 in Song (2023) to identify key tracers during incense burning (Song et al. 2023). Nevertheless, the



75 interpretation of GC×GC-MS data demands advanced computational tools and expertise, and the
76 investigation of unknown compounds remains scarce due to the inadequate validation procedures,
77 overreliance on manual data processing, limited access to computational capabilities, and the lacked
78 expertise to handle the complex chromatographic data effectively.

79 Bridging this gap requires further development of sophisticated algorithms and analytical approaches to
80 unlock the full potential of GC×GC. This study proposed a bottom-up method for cluster analysis and
81 quantification of organic vapours and aerosols within complex atmospheric mixtures. The scripts were
82 initiated with the recognition of the common mass spectra features of specific species and tailored to a
83 wide range of compound clusters. The scripts were then trained, iterated, and optimized incorporating
84 real sample data until robust outputs were achieved. The new strategy reduced the ambiguity that is often
85 associated with identifying compounds in complex mixtures.

86 The proliferation of heavy-duty diesel vehicles (HDDVs) has raised significant concerns, with an
87 escalating demand for freight transport and in various industrial operations (Yan et al. 2022, Cheng et al.
88 2022). Despite a low retention rate, HDDVs release massive amounts of particulate matter, nitrogen
89 oxides, ammonia, and carbon monoxide into the atmosphere, compared with other vehicle types (Wang
90 et al. 2023, Silva et al. 2023, Chang et al. 2022, Stanimirova et al. 2023, Hamilton and Harley 2021,
91 2021, Krueve et al. 2014). Given this, the gas and aerosol samples from representative HDDV tailpipes
92 and the ambient environment were collected and analyzed by GC×GC-MS. The proposed bottom-up
93 method was applied for a comprehensive analysis of the complex organic mixtures, resolving 26
94 compound categories including hydrocarbons in multiple forms, oxygenated components, and
95 heteroatom containing species. Over 80% of all the chromatographic peaks were identified and assigned
96 to a compound cluster using proposed method, leaving a minor portion of organic matrix unresolved.
97 Different compound clusters occupied separate positions in the GC×GC space, and distinctive
98 distribution patterns within diverse samples and their contribution fractions were revealed. Quantification
99 uncertainties were addressed thoroughly and the significant potential deviation when using n-alkanes as
100 semi-quantification surrogates was proved. Overall, the integration of automated algorithms and GC×GC
101 data analysis holds significant implications for advancing our understanding of atmospheric chemistry,
102 improving secondary organic aerosol (SOA) estimation, and thus guiding the implementation of
103 environmental policies.



104 **2 Materials and methods**

105 **2.1 Sample collection, treatment, and instrumental analysis**

106 For the collection of HDDVs tailpipe emission, chassis dynamometer experiments were conducted at the
107 China Automotive Technology & Research Center (CATARC) in Guangzhou, China. Exhaust emissions
108 from HDDVs were diluted in a constant volume sampler (CVS, CVS-ONE-MV-HE, Horiba), following
109 the China heavy-duty commercial vehicle test cycle for tractor trailers (CHTC-TT) driving cycles. The
110 average temperature in the sampling train was precisely controlled at 47 °C, and airflow, relative
111 humidity, and airflow, relative humidity, and pressure were monitored simultaneously. The speed trace
112 and characteristics of CHTC-TT are shown in Figure S1.

113 Gaseous exhausts were collected by two adsorbent thermal desorption (TD) tubes in series (Tenax TA,
114 C1-AXXX-5003, Markes International) after being filtered by a Teflon filter. Particulate exhausts were
115 deposited on a 47 mm quartz filter (Grade QM-A, Whatman). Ambient PM_{2.5} filter samples were
116 collected on the rooftop of a 5-story building on the campus of Shenzhen University (22.60°N, 114.00°E)
117 in western Shenzhen, approximately 25 m above the ground. The sampling site was surrounded by
118 campus, residential areas, greenbelts, and a golf park and, the location map is shown in Figure S2.
119 Previous studies demonstrated that the PM_{2.5} concentration in this area represented the average pollution
120 scheme in Shenzhen (Huang et al. 2018, Yu et al. 2020). Sampling strategy followed a regular schedule
121 of one 24-h sample every day using a high-volume sampler (Th-1000c II, Wuhan Tianhong
122 Environmental Protection Industry Co., Ltd). TD samples were kept dry at room temperature, and quartz
123 filters were stored frozen at -18 °C before analysis. All sampling materials were pre-baked thoroughly
124 to remove potential carbonaceous contamination.

125 TD samples were injected with 2 µL of deuterated internal standard (IS) mixing solution through a mild
126 N₂ blow (CSLR, Markes International). A precious portion of 1 cm² (1 cm × 1 cm) filter sample was
127 isolated and cut into strips. They were spiked with 2 µL of IS mixing solution and inserted into a
128 passivated quartz tube. All TD samples and quartz tubes were loaded onto a thermal desorption
129 autosampler (ULTRA-xr, Markes International), thermally desorbed (UNITY-xr, Markes International),
130 and subjected to GC×GC separation (Agilent 8890, Agilent Technologies; Solid State Modulator1810,
131 J&X Technologies) and mass spectrometry detection (Agilent 5977B, Agilent Technologies).



132 The thermal desorption system heated the TD tubes to 320 °C (quartz tubes to 330 °C) for 20 min, while
133 the trap remained at 20 °C. Following tube desorption, the trap temperature was raised to 330 °C (340
134 °C for quartz tubes measurement) for 5 min at the maximum heating rate, and the vaporized analytes
135 were purged into the 1st GC column with a desorb split flow of 6 mL/min. Separation of the analytes was
136 carried out using a DB-5ms capillary column (30 m × 0.25 mm × 0.25 μm, Agilent Technologies) as the
137 primary column and a DB-17MS capillary column (1.2 m × 0.18 mm × 0.18 μm, Agilent Technologies)
138 as the secondary column. The modulation column consisted of a VF-1MS capillary column (0.7 m × 0.25
139 mm × 0.10 μm, Agilent Technologies) connecting to the 1st column and an Ultimate Plus deactivated
140 fused silica tubing (0.6 m × 0.25 mm, Agilent Technologies) connecting to the 2nd column.
141 Initially, the GC oven was set at 50 °C for a 3-min duration, followed by a gradual increase at a rate of 5
142 °C/min until it reached 310 °C, where it was maintained for an additional 5 minutes. The entry and exit
143 hot zones were +10 °C higher than the GC oven temperature, and the trap zone was maintained at -50
144 °C. The modulation cycle had a period of 4 s. Carrier gas flow was set at 1.2 mL/min. The ion source
145 was kept at 250 °C and scanned over a range of 20 – 350 amu.

146 **2.2 Data collection, alignment, and parsing**

147 GC×GC-MS data acquisition was conducted using Enhanced MassHunter (version 10.0, Agilent
148 Technologies) and SSCenter (version 2.4.0.0, J&X Technologies). All data utilized to develop and test
149 the scripts were processed by Canvas Browser (version 2.5, J&X Technologies) for basic preprocessing,
150 such as baseline correction, mass spectra deconvolution, and peak smoothing. The application of baseline
151 correction and peak smoothing allowed for an increased signal-to-noise ratio (S/N) and improved overall
152 data quality. Chromatographic peaks were filtered according to the filtering rules: baseline noise = 150,
153 S/N > 50. For each individual sample, after isolating all compounds of interest, a peak table in 1st
154 retention time (RT) sequential order with 1st RT and 2nd RT, peak area, peak height, peak width, and
155 deconvoluted mass spectra was exported. These quantitative variables were further processed for targeted
156 and non-targeted “omics” oriented analysis.

157 As anticipated, the chromatographic variables experienced RT shifts due to column degradation, routine
158 maintenance (e.g., cutting column), and system fluctuation (e.g., carrier gas pressure variation). The
159 initial RT shifting tolerance for adaptive cluster matching was set to be 1 period of modulation in the 1st
160 dimension and 0.1 s in the 2nd dimension. Additionally, a 2D shift cluster consisting of C₁₆D₃₄, C₂₄D₅₀,



161 and C₃₂D₆₆, with the merit of correcting 2nd RT shift, was configured. Data correction or data alignment
162 is crucial for accurate and consistent peak integration.

163 **2.3 Algorithmic development**

164 EI spectra are typically characterized by a molecular ion (M⁺) peak plus a collection of fragment ion
165 peaks. The M⁺ may dominate the mass spectrum in some cases (e.g., un-substituted polycyclic aromatic
166 hydrocarbons (PAHs)), and more frequently presents at a relatively low intensity. The EI spectra are
167 highly comparable among different instrument systems and experimental conditions, making them an
168 excellent measure to identify compounds. The characteristic ions and their relative intensities depend on
169 the intrinsic nature of the targeted compounds, necessitating knowledge of basic rules and common
170 fragmentation routes to interpret EI mass spectra. Figure 1 illustrates the workflow for establishing
171 computational strategies for robust and reproducible GC×GC-MS data processing.

172 Functional groups have significant effects the fragmentation patterns observed in mass spectrometry, and
173 some ions are typical of given structures. Isotopic peaks (e.g., hydrogen and chlorine) provide additional
174 information about the molecules (Du and Angeletti 2006, Fernandez-de-Cossio et al. 2004). These pieces
175 of information formed the foundation for building up the model for cluster analysis and are addressed in
176 greater detail in the supporting information (S1). These indicative reaction schemes have been
177 incorporated into the model development. Each critical step of model construction and validation is
178 described thoroughly. The quantitative variables in the data alignment table, combining the
179 chromatographic and MS information are properly exploited and determine the overall speciation
180 capacities. Traditionally, compound identification relies on the electron ionization-based fragmentogram
181 and the deconvoluted mass spectra. Empirically speaking, one-by-one compound identification would
182 be greatly intervened by neighbouring peaks, especially those with similar structures, and introduce
183 considerable uncertainties. A good example is the assignment of homologous *n*-alkanes, of which the
184 fragmentogram bears a close resemblance (Figure S5). In such cases, the similarity score (the measure
185 of similarity between the observed mass spectrum and the NIST library hit) could be erroneously inflated
186 to 850 (out of 999) or higher. In contrast, cluster analysis or “omics” oriented analysis involves the
187 comprehensive analysis of a specific type of compounds on a large scale, aiming to provide a holistic
188 understanding of the distribution and transformation of the specific compound cluster being investigated.



189 Due to the complexity and remarkable peak capacities, sophisticated and detailed scripts for cluster
190 identification were constructed. Heteroatom containing species, e.g., amides and amines, were carefully
191 examined. The scripts began by recognition of the common mass spectra features of compound cluster
192 of interest and are addressed in more details as follows:

- 193 1. The Boolean value of characteristic ions.
- 194 2. The intensity sequence of abundant ions in the whole spectra.
- 195 3. The retention time window restriction for certain compound groups.
- 196 4. The pattern of mass spectrometry variation with the increased number of substituents or the
197 extension of the carbon chain.
- 198 5. Iteration framework that involved repetitive cycles among all the tested samples.

199 The scripts were then trained, iterated, and optimized incorporating real sample data, and the parameters
200 were adjusted accordingly until a robust output was achieved. The extractor function built in the Canvas
201 software was activated, and all the scripts were imported to facilitate automated cluster analysis. The
202 scripts parsed all the files in the given directory into the required structure and generated three reports in
203 the form of .pdf, .csv, and .bmp. The .csv file contained key information including the compound name,
204 compound cluster, 1st and 2nd RTs, and peak area (based on total ion current (TIC)).

205 Once exported, the peaks were further processed for quantification/semi-quantification following the
206 steps below. First, calibration curves were prepared by spiking different volumes of the standard solution
207 mixture onto the blank TD tubes and blank filters, respectively. Peak area ratios, i.e., peak area of
208 authentic standards over that of the internal standards, were used to build the linear relationship, with the
209 merit of correcting system fluctuation. The selection of authentic standards prioritizes their wide
210 distribution across the entire chromatogram space, ranging from high to low volatility and weak to strong
211 polarity, and meanwhile encompassing a broader range of functional groups and heteroatoms. The
212 distribution and performance of all authentic standards are summarized in Table S1 and Figure S6.
213 Second, for the un-quantified peaks, their complied information (X, Y, Z) corresponding to (1st RT, 2nd
214 RT, compound cluster) is looped through the list of all authentic standards in the following descriptive
215 algorithm framework (note that the statements do not conform to the grammar rule and it is for illustrative
216 purpose only) until the optimal authentic standard to semi-quantity the target peaks is exported. It should
217 be emphasized that the un-quantified peak and the corresponding authentic standards to semi-quantify it
218 must belong to the same group, due to their physics-chemical similarities.



```

For (i = 1 to n) # n equals the number of authentic standards and is a known variable.

    If (ZM = Zi) # M is the un-quantified peak and i refers to the authentic standard that is selected in
a certain loop.

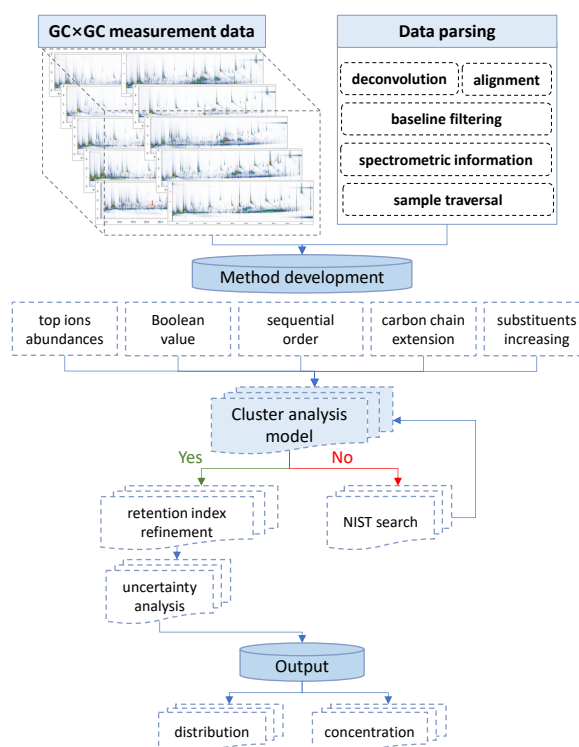
        Ai = Min (an array of ((XM - Xi)2 + (YM - Yi)2)) # This sentence dose not conform to the
grammar rule of Visual Basic for Applications in Excel, and it is for illustrative purpose only.

        Export Zi, (Xi, Yi, Zi), its peak area, and its linear calibration relationship.

    End if

Next i
    
```

219



220

221

222

Figure 1. Flow diagram illustrating the multistep data processing for establishing computational strategies for cluster analysis and quantification of organic vapours and aerosols using GCxGC-MS data.

223

2.4 Quality assurance/control and uncertainty evaluation

224

It is common for thermal decomposition to occur in analytical methods involving heating processes,

225

potentially leading to the erroneous detection of compounds that are either not present in real samples or



226 present in low concentrations. Such artifacts need careful scrutiny, and the availability of authentic
227 standards covering the GC×GC space range is essential for validation. The thermal programs used in this
228 study were highly similar to those employed by Franklin (2023), who observed low chromatographic
229 signals of decomposition products (Franklin et al. 2023). Nevertheless, the possibility that some observed
230 analytes are decomposition products cannot be entirely ruled out. Peaks of ISs were traced across all
231 samples to monitor the variation of several modules, and the results are presented in Figure S7. Excellent
232 stability was clearly observed, demonstrating the robustness of the testing system. Strong linear
233 correlations were achieved for this set of authentic standards, with Pearson's R ranging from 0.97 to
234 0.99. Routine blank tests were conducted to prevent unexpected contamination.

235 **3 Results and discussion**

236 **3.1 Overall performance of the algorithm and compound identification**

237 The optimization of component identification remains a challenging issue, and this work involves
238 converting known chemical compounds into molecular descriptors and utilizing cluster analysis to
239 predict the relationship between these descriptors and structural information. After continuous trials to
240 improve reliability and data processing speed, a final solution of 26 compound clusters stands out with
241 high accuracy and repeatability:

- 242 – Aliphatic hydrocarbons, including *n*-*i*- alkanes and alkenes
- 243 – Cycloalkanes
- 244 – Alkyl-substituted benzenes, including C₁ – C₆ alkyl-substituted benzenes
- 245 – Admantanes
- 246 – Hopanes
- 247 – 2 – 5 ring PAHs
- 248 – Acids
- 249 – Aliphatic alcohols
- 250 – Aliphatic aldehydes and ketones
- 251 – Oxy-PAHs
- 252 – Phthalates
- 253 – Phenols and alkyl-substituted phenols



254 – Phenol ethers

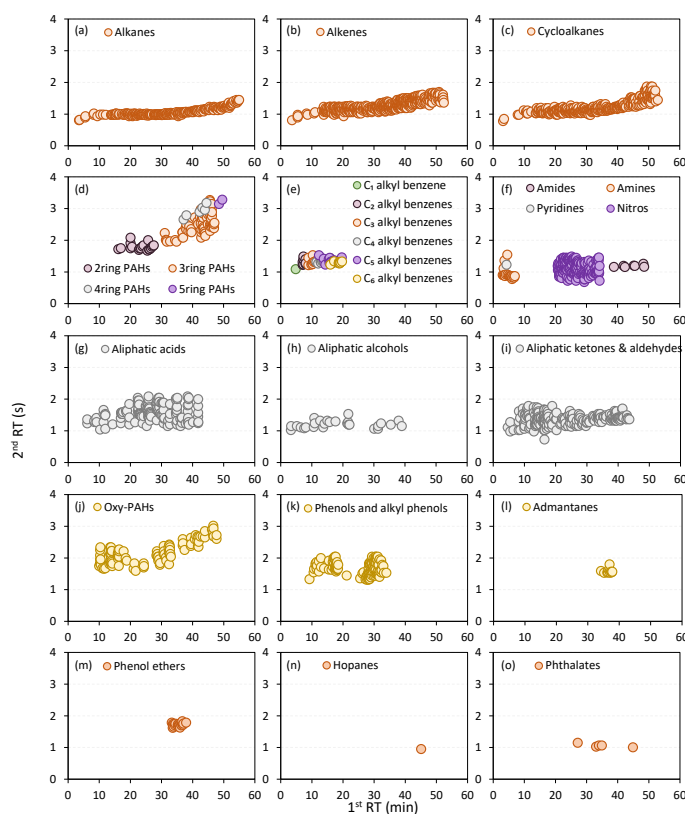
255 – Amides

256 – Amines

257 – Pyridines

258 – Nitros, including organic nitrates and organic nitrites

259 Validation of the model output using field diesel samples has been conducted and has shown high
260 estimation accuracy and integrity. Generally, over 82% of the peaks have been successfully classified
261 and assigned to the corresponding compound groups and their distribution in an example GC×GC plot
262 is shown in Figure 2. To confirm the tentatively identified heteroatom groups, their raw chromatogram,
263 mass spectra, and chemical structures of representative species are displayed in Figures S9-S15. Less
264 than 18% of the chromatographic peaks were identified as unresolved components. Basically, aliphatic
265 hydrocarbons were located in the lowest position in a GC×GC space except column bleedings (Figure
266 2a-c and Figure S8), and their 2nd RT drift was less than 1s from the far-left to the far-right side. N-
267 containing compounds in oxidized and reduced valences, including amides, amines, pyridines, and nitros,
268 were resolved simultaneously under respective filtering rules, and they occupied a slightly higher
269 position in the GC×GC space (Figure 2f). Amines and pyridines were more volatile species and eluted
270 at early stages, whereas nitros and amides were eluted at middle and late stages sequentially. Due to their
271 high volatility, C₂-C₆ alkyl-substituted benzenes also presented at the beginning of the GC×GC space
272 and they partitioned dominantly into the gas phase. Their 2nd RTs were comparable to those of pyridines
273 and amides, and the 2nd RT drift was negligible. Aliphatic O-containing compounds, including acids,
274 alcohols, and ketones, were found to be in the middle region and covered a wide volatility rang. Aliphatic
275 O-containing compounds affect the acidity of the atmosphere, participate in aqueous phase reactions, and
276 contribute significantly to the formation of SOA (Cope et al. 2021, Xu et al. 2022). Phenols with one or
277 more hydroxyl groups attached to an aromatic benzene ring were observed in the middle of the GC×GC
278 space. Oxy-PAHs and PAHs presented in the upper middle of GC×GC space, and the volatility range
279 stretched to the low volatility end, for which a clear trend tilting to the upper right corner was observed,
280 suggesting that the aromaticity played a significant role in the retention in the secondary dimension.



281

282 **Figure 2.** The distribution of the 26 compound groups in an example GCxGC plot. For clear visualization,
 283 different compound groups are displayed separately, except for 2 – 5 ring PAHs, C₂ – C₆ alkyl-substituted
 284 benzenes, and N-containing species. Nitros include organic nitrates and organic nitrites, due to the co-
 285 existence of the characteristic ions at m/z 30 (NO⁺) and m/z 46 (NO₂⁺).

286 3.2 Model uncertainty estimation

287 We conducted a systematic evaluation of the model output, and the results are shown in Figure 3 and
 288 Figure 4. To address this issue comprehensively and accurately, we selected three types of standards
 289 including C₇ – C₃₇ *n*-alkanes, C₂ – C₆ alkyl-substituted benzenes, and 2 – 4 ring PAHs, representing a
 290 full range of low to high polarity and various functionalities. The quantification deviation was computed
 291 according to the principles of the model. Chromatographic peaks were quantified by either their authentic
 292 standards or the surrogates that fell within the same compound category after being classified to one of
 293 the 26 compound classes. For example, if the mass spectrum of a chromatographic peak followed the
 294 pattern of the compound class of alkanes, it would be assigned into the alkane group and quantified by
 295 its authentic standard if any, or by the *n*-alkane (*n*-alkane serving as the semi-quantification surrogate in



296 this case) that was closest to it spatially. Similarly, if the mass spectrum of a chromatographic peak
297 followed the pattern of C_x alkyl-substituted benzenes, it would be assigned into the C_x alkyl-substituted
298 benzene group and quantified by its authentic standard if any, or by the alkyl-substituted benzene (alkyl-
299 substituted benzenes serving as the semi-quantification surrogate) that was closest to it spatially. In light
300 of the explanation, the deviation of the slopes of the calibration curves of any pair of the adjacent
301 authentic standards that fell within the same compound category was computed to represent the ceiling
302 of the semi-quantification uncertainty. Uncertainties are computed using the following Eq. (1):

$$303 \text{ Uncertainty (\%)} = \frac{\text{Abs}(S_p - S_s)}{\text{Smaller}(S_p, S_s)} * 100 \quad (1)$$

304 where S_p and S_s are the slopes of the previous and subsequent compounds, respectively.

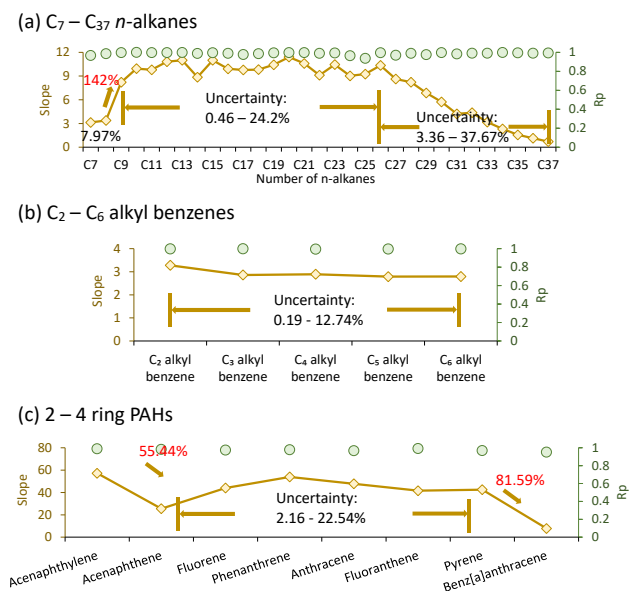
305 The slopes increased rapidly from 3.13 (C_7 *n*-alkane) to 8.21 (C_9 *n*-alkane), fluctuated slightly from 8.85
306 to 11.8 in the range of C_9 to C_{27} *n*-alkanes, and decreased gradually after C_{28} *n*-alkane to the end of C_{37}
307 *n*-alkane. In the whole volatility range of C_9 – C_{37} *n*-alkanes, the uncertainties were less than 37.67%,
308 except for one time interval between C_8 and C_9 *n*-alkanes, where the quantification deviation reached
309 142%. A similar trend was observed for PAHs, with uncertainties less than 22.54%, except for the first-
310 and last-time intervals, where the quantification deviations were 55.44% and 81.59%, as shown in Figure
311 3. Stable responses of C_2 – C_6 alkyl-substituted benzenes were monitored, and the uncertainties were less
312 than 12.74%. In other words, for any given peak, it would be quantified/semi-quantified by one authentic
313 standard, and the upper limit of quantification uncertainty originated from any pair of the adjacent
314 authentic standards was as discussed earlier.

315 It made sense that the uncertainty ranges of alkyl-substituted benzenes were less than those of *n*-alkanes
316 and PAHs, given that alkyl-substituted benzenes were eluted early at the front half, whereas alkanes and
317 PAHs covered the whole volatility range. The trends illustrated that the responses of GC×GC to the
318 analysts were sensitive to the volatility distribution and region for accurate quantification fell in the
319 middle part. It also highlighted the utility of introducing more authentic standards and the benefits of
320 enriching compound categories. We could speculate that the quantification uncertainty would be further
321 reduced with the augmentation of standard compounds.

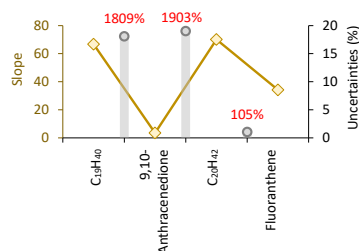
322 Furthermore, we delved into the uncertainty estimation of dividing the whole chromatogram into bins
323 based on retention time, and all the species in the same bin were quantified, referring to the mass-to-
324 signal responses of the C_n *n*-alkanes (Zhao et al. 2015, Zhao et al. 2014). This approach corrected the



325 signal variation of hydrocarbons in the GC-MS and was widely adopted for quantifying unresolved
 326 complex mixtures (UCMs) (Shen et al. 2023, Zhao et al. 2022). We chose four types of standards
 327 belonging to different compound categories with similar 1st RTs and different 2nd RTs, including C₁₉H₄₀
 328 (1st RT = 34.6 min, 2nd RT = 1.03 s), 9,10-anthracenedione (1st RT = 36.07 min, 2nd RT = 3.85 s), C₁₉H₄₀
 329 (1st RT = 36.54 min, 2nd RT = 1.07 s), and fluoranthene (1st RT = 37.00 min, 2nd RT = 3.04 s), and
 330 assessed the deviation of slopes of each pair of the standards. Results in Figure 4 show that the deviation
 331 between the three pairs of standards was 1809% (C₁₉ *n*-alkane vs. 9,10-anthracenedione), 1903% (9,10-
 332 anthracenedione vs. C₂₀ *n*-alkane), and 105% (C₂₀ *n*-alkane vs. fluoranthene), respectively. The
 333 quantitative errors in quantifying unidentified chromatographic peaks using responses of *n*-alkanes could
 334 reach three orders of magnitude, especially for O-containing species, and those errors in quantifying
 335 aromatic components, e.g., PAHs, also exceeded 100% in some cases.



336
 337 **Figure 3.** Slope and Pearson correlation variation of (a) C₇ – C₃₇ *n*-alkanes, (b) C₂ – C₆ alkyl-substituted
 338 benzenes, and (c) 2 – 4 ring PAHs. Brown diamond dots represent slopes of different species and are
 339 referenced to the left-axis. Green circles denote the Pearson correlation of individual species and are
 340 referenced to the right-axis. Pearson correlation values of *n*-alkanes, C₂ – C₆ alkyl-substituted benzenes, and
 341 2 – 4 ring PAHs range from 0.936 to 0.999, 0.994 to 0.998, and 0.952 to 0.992, respectively. Uncertainties are
 342 computed using the equation provided in the main text.



343
344 **Figure 4. Slopes and uncertainty estimation of example compounds with close 1st RTs and different 2nd RTs:**
345 **C₁₉H₄₀ (1st RT = 34.6 min, 2nd RT = 1.03 s), 9,10-anthracenedione (1st RT = 36.07 min, 2nd RT = 3.85 s), C₂₀H₄₂**
346 **(1st RT = 36.54 min, 2nd RT = 1.07 s), and fluoranthene (1st RT = 37.00 min, 2nd RT = 3.04 s). Brown diamond**
347 **dots represent slopes of different species and are referenced to the left-axis. Gray bars denote the uncertainty**
348 **estimation of example compounds and are referenced to the right-axis.**

349 3.3 Cluster analysis in organic vapor and aerosol samples

350 The model was applied to organic vapor samples from HDDV tailpipe emission (HDDV vapours for
351 short), aerosol samples from HDDV tailpipe emission (HDDV aerosols for short), and atmospheric
352 aerosol samples (ambient aerosols for short) for cluster analysis. The results are shown in Figure S16,
353 displaying the top few species' distribution with a contribution fraction exceeding 5%, and in Figure 5,
354 showing the mass stacking. Overall, the speciated chromatographic peaks accounted for 85%, 82%, and
355 99% for HDDV vapor, HDDV aerosol, and ambient aerosol samples, respectively. The unidentified
356 peaks were less than 20% and addressed in greater details in the supporting information (S1).

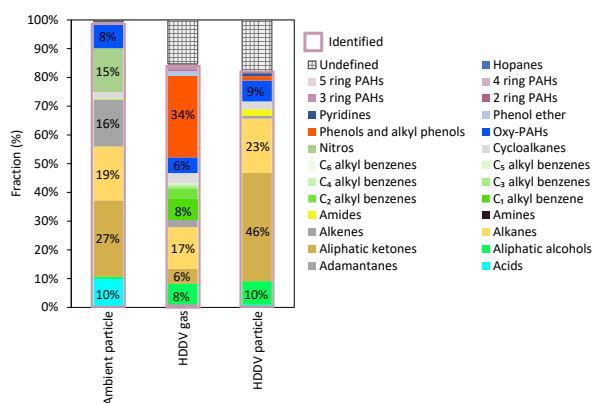
357 Distinct cluster distribution features could be extracted. For ambient aerosol samples, six compound
358 clusters were filtered, and aliphatic ketones were the most abundant cluster, contributing to 27% of all
359 the peak signals, followed by alkanes and alkenes. A notable fraction of 15.2% of organic nitros was
360 observed in ambient samples exclusively, indicating significant secondary nitrate formation processes
361 under atmospheric conditions. Aliphatic acids and oxy-PAHs were also detected at an abundant level,
362 and the top six groups accounted for over 95% of the total classified peak signals. Minor but non-
363 negligible fractions included cycloalkane, aliphatic alcohols, and phenols and alkyl-substituted phenols.
364 Similarly, aliphatic ketones ranked first for HDDV aerosol samples, with the mass intensity reaching
365 46% of the total signals, followed by alkanes. Aliphatic alcohols and oxy-PAHs were detected at an
366 abundant level, and the top four groups accounted for over 88% of the total classified peak signals.
367 Cycloalkanes, amides, phenols and alkyl-substituted phenols, and alkenes were compound clusters with
368 lower abundance ranging from 1-4%.



369 For HDDV vapours, the most abundant group was phenols and alkyl-substituted phenols, constituting
370 34% of the total peak signals. Compared with previous results where the most abundant group was
371 reported to be alkanes,(Wang et al. 2022, Alam et al. 2019) the adoption of the innovative model
372 contributed to resolving the oxygenated fractions and reduced inaccuracies in SOA simulation due to the
373 lack of species information. The compound cluster is confirmed by 1) the retention time window
374 including 1st RT and 2nd RT, and 2) the mass spectra. Detailed information is displayed in Figure S15.
375 The 2nd RTs of the identified phenols and alkyl-substituted phenols range from 1.45 to 1.78 s, well above
376 the hydrocarbon regions, of which the 2nd RTs fall within the range of 1.0 to 1.15 s approximately. Their
377 mass spectra also feature with the typical phenol ions at $m/z = 94, 107, 121, 135, 149,$ and 191. Alkanes
378 ranked as the second top species, followed by C₁ alkyl-substituted benzene. C₁ – C₆ alkyl-substituted
379 benzenes were negligible in both ambient and HDDV aerosol samples, whereas in notable abundance in
380 HDDV vapor samples. This distribution aligned with their placement in the GC×GC plot, indicating they
381 were relatively volatile species and partitioned predominantly into the gas phase. Oxy-PAHs and
382 aliphatic ketones contributed to 6% of the total identified peak intensities, followed by some minor
383 fractions, including C₂ alkyl-substituted benzene, cycloalkanes, and alkenes.
384 The model output illustrates the overall distribution of compound clusters in various gas and aerosol
385 samples, providing comparative insights. Carboxylic acids indicated a higher oxidation state than other
386 compound clusters and were exclusively observed at a notable level in ambient samples compared with
387 “freshly emitted” source samples. The oxidation state of dominant compounds in HDDV samples was
388 comparatively low. For example, a significant ketone fraction was observed in HDDV samples, with the
389 majority partitioning into the aerosol phase due to the long chain carbon skeleton and thus low volatility.
390 Phenols and alkyl-substituted phenols were the leading species in HDDV gas samples. He (2022)
391 reported that the oxygenated I/SVOCs accounted for over 20% of the total I/SVOCs mass in HDDV
392 tailpipe emissions (He et al. 2022a). With the refinement and improvement of model performance, e.g.,
393 further splitting mixed mixtures, the oxygenated fraction was elevated to over 50%.
394 This study highlighted the systematic presence and distribution of N-containing compounds in oxidized
395 valences (including nitros) and reduced valences (including amides, amines, pyridines). Among them,
396 amines and amides were key precursors for new particle formation processes in a polluted atmosphere
397 (Saeki et al. 2022, Cai et al. 2021), and pyridines, with the N atom in the aromatic ring, were readily
398 dissolved in water, participating in the global N cycle in ecosystems (Kosyakov et al. 2020). Nitros



399 covered a wide range of organic compounds with NO or NO₂ substituents and served as critical tracers
 400 for secondary nitrate formation processes. Amines and pyridines were volatile species occupying the
 401 early section of the GC×GC space, while nitros and amides were distributed in the middle and rear space.
 402 Individual N-containing species were at trace levels under atmospheric conditions and were hardly
 403 detectable. Moreover, authentic standards or high-resolution mass spectrometry were required to identify
 404 and quantify each compound (Zhang et al. 2018). With the establishment of an algorithmic solution, we
 405 were able to conduct a full scan of N-containing compound clusters.
 406 In addition to common features, specific compounds were identified in separate samples and could
 407 potentially serve as markers or tracers for primary emission. Adamantane and its derivatives, with the
 408 fusion of three cyclohexane rings (chemical structure and mass spectrum shown in Figure S17a), were
 409 natural products in petroleum (Stout and Douglas 2004). They were volatile and had previously been
 410 isolated using GC×GC-ToF-MS in crude oil (Wang et al. 2013). Adamantanes were observed in HDDV
 411 vapor samples, contributing 1.4% to the identified peaks. Hopane (chemical structure and mass spectrum
 412 shown in Figure S17b) was also a natural product in petroleum and bitumen, and it was an important
 413 marker for vehicle emissions due to its persistency and stability (He et al. 2022b, Wong et al. 2021).
 414 Hopane was reported to survive heat treatment up to 460 °C and was exclusively detected in HDDV
 415 aerosol samples, with an intensity fraction of 0.3% (Wu and Geng 2016).



416

417 **Figure 5. The fraction distributions of different compound clusters in ambient aerosol samples, HDDV**
 418 **tailpipe vapours, and HDDV tailpipe aerosols. Numbers labelled on each column represent the fractions of**
 419 **the top few groups in different samples. Identified clusters are outlined in light purple.**



420 **4 Conclusions and outlook**

421 We presented an innovative method for optimizing the separation and identification of organic vapours
422 and aerosols, with a focus on establishing molecular descriptors and cluster analysis algorithms. The
423 model outputs were validated using field samples with high accuracy and integrity. Less than 20% of the
424 peaks were unresolved components. The retention patterns of various compound groups and their
425 distribution in the GC×GC plot were resolved, and the influence of functional groups on fragmentation
426 was thoroughly addressed. We also provided a comprehensive analysis of the quantification uncertainties
427 of this new approach and highlighted the significant quantitative errors when using *n*-alkanes as semi-
428 quantification surrogates. This model was applied to various types of field samples, and the results
429 revealed distinctive distribution patterns of compound clusters and contribution fractions, providing
430 valuable insights into the compositions of organic vapours and aerosols, and offering potential markers
431 for specific emission sources.

432 Compound speciation in atmospheric chemistry continues to be a dynamic and challenging field.
433 Speciated compounds enable models to consider the diversity of organic species and dynamic chemical
434 transformation in the atmosphere, contributing to more accurate SOA simulation results. It also allows
435 for a more refined description of the dispersion of pollutants, thereby assisting in the development of
436 localized air quality management strategies, as we strive for a more accurate and broad understanding of
437 atmospheric chemistry.



438 **Supplement link:**

439 **Author contribution:**

440 X.H.: Conceptualization, formal analysis, model development, data validation, writing—original draft,
441 funding acquisition; X.Z.: Writing—reviewing and editing, project administration, supervision, funding
442 acquisition; S.G: Experiment; L.Z., T.C., B.Y., and S.X.: Experiment; Q.W., Z.L., Y.Y., S.Z., and Y.W.:
443 Data validation, writing—reviewing and editing.

444 **Competing interests:**

445 The authors declare that they have no conflict of interest.

446 **Acknowledgements**

447 The authors acknowledge the financial support of the National Natural Science Foundation of China
448 (Grant No. 42105100 and 42261160645), Scientific Research Fund at Shenzhen University (868-
449 000001032089 and 827-000907), and Macao Science and Technology Development Fund
450 (0023/2022/AFJ).

451 **References**

- 452 2021. Ministry of Ecology and Environment of the People's Republic of China. China Mobile Source
453 Environmental Management Annual Report 2021.
- 454 Alam, M. S., C. E. West, A. G. Scarlett, S. J. Rowland & R. M. Harrison Application of 2D-GCMS
455 reveals many industrial chemicals in airborne particulate matter. *Atmospheric Environment*, 65, 101-111,
456 2013.
- 457 Alam, M. S., S. Zeraati-Rezaei, H. M. Xu & R. M. Harrison Characterization of Gas and Particulate
458 Phase Organic Emissions (C₉-C₃₇) from a Diesel Engine and the Effect of Abatement Devices.
459 *Environmental Science & Technology*, 53, 11345-11352, 2019.
- 460 Bendik, J., R. Kalia, J. Sukumaran, W. H. Richardot, E. Hoh & S. T. Kelley Automated high confidence
461 compound identification of electron ionization mass spectra for nontargeted analysis. *J Chromatogr A*,
462 1660, 462656, <https://www.ncbi.nlm.nih.gov/pubmed/34798444>, 2021.
- 463 Cai, R. L., C. Yan, D. R. Worsnop, F. Bianchi, V. M. Kerminen, Y. C. Liu, L. Wang, J. Zheng, M.
464 Kulmala & J. K. Jiang An indicator for sulfuric acid-amine nucleation in atmospheric environments.
465 *Aerosol Science and Technology*, 55, 1059-1069, 2021.
- 466 Chang, Y. H., K. Cheng, Y. Q. Kuang, Q. Y. Hu, Y. Q. Gao, R. J. Huang, C. Huang, W. W. Walters &
467 M. F. Lehmann Isotopic Variability of Ammonia ($\delta^{15}\text{N-NH}_3$) Slipped from Heavy-Duty Vehicles under
468 Real-World Conditions. *Environ Sci Technol Letters*, 9, 726-732, 2022.



- 469 Cheng, S. F., Y. B. Zhao, B. B. Zhang, P. Peng & F. Lu Structural decomposition of heavy-duty diesel
470 truck emission contribution based on trajectory mining. *Journal of Cleaner Production*, 380, 135172,
471 2022.
- 472 Cope, J. D., K. A. Abellar, K. H. Bates, X. Fu & T. B. Nguyen Aqueous Photochemistry of 2-Methyltetrol
473 and Erythritol as Sources of Formic Acid and Acetic Acid in the Atmosphere. *ACS Earth and Space*
474 *Chemistry*, 5, 1265-1277, <https://doi.org/10.1021/acsearthspacechem.1c00107>, 2021.
- 475 Du, P. & R. H. Angeletti Automatic deconvolution of isotope-resolved mass spectra using variable
476 selection and quantized peptide mass distribution. *Anal Chem*, 78, 3385-3392,
477 <https://www.ncbi.nlm.nih.gov/pubmed/16689541>, 2006.
- 478 Fernandez-de-Cossio, J., L. J. Gonzalez, Y. Satomi, L. Betancourt, Y. Ramos, V. Huerta, V. Besada, G.
479 Padron, N. Minamino & T. Takao Automated interpretation of mass spectra of complex mixtures by
480 matching of isotope peak distributions. *Rapid Commun Mass Spectrom*, 18, 2465-2472,
481 <https://www.ncbi.nlm.nih.gov/pubmed/15384131>, 2004.
- 482 Franklin, E. B., S. Amiri, D. Crocker, C. Morris, K. Mayer, J. S. Sauer, R. J. Weber, C. Lee, F. Malfatti,
483 C. D. Cappa, T. H. Bertram, K. A. Prather & A. H. Goldstein Anthropogenic and Biogenic Contributions
484 to the Organic Composition of Coastal Submicron Sea Spray Aerosol. *Environ Sci Technol*, 56, 16633-
485 16642, <https://www.ncbi.nlm.nih.gov/pubmed/36332100>, 2022.
- 486 Franklin, E. B., L. D. Yee, R. Wernis, G. Isaacman-VanWertz, N. Kreisberg, R. Weber, H. Zhang, B. B.
487 Palm, W. Hu, P. Campuzano-Jost, D. A. Day, A. Manzi, P. Artaxo, R. A. F. Souza, J. L. Jimenez, S. T.
488 Martin & A. H. Goldstein Chemical Signatures of Seasonally Unique Anthropogenic Influences on
489 Organic Aerosol Composition in the Central Amazon. *Environ Sci Technol*, 57, 6263-6272,
490 <https://www.ncbi.nlm.nih.gov/pubmed/37011031>, 2023.
- 491 Guo, Q., J. Yu, K. Yang, X. Wen, H. Zhang, Z. Yu, H. Li, D. Zhang & M. Yang Identification of complex
492 septic odorants in Huangpu River source water by combining the data from gas chromatography-
493 olfactometry and comprehensive two-dimensional gas chromatography using retention indices. *Sci Total*
494 *Environ*, 556, 36-44, <https://www.ncbi.nlm.nih.gov/pubmed/26974564>, 2016.
- 495 Hamilton, S. D. & R. A. Harley High-Resolution Modeling and Apportionment of Diesel-Related
496 Contributions to Black Carbon Concentrations. *Environ Sci Technol*, 55, 12250-12260, 2021.
- 497 He, X., X. Zheng, Y. You, S. Zhang, B. Zhao, X. Wang, G. Huang, T. Chen, Y. Cao, L. He, X. Chang,
498 S. Wang & Y. Wu Comprehensive chemical characterization of gaseous I/SVOC emissions from heavy-
499 duty diesel vehicles using two-dimensional gas chromatography time-of-flight mass spectrometry.
500 *Environ Pollut*, 305, 119284, <https://www.ncbi.nlm.nih.gov/pubmed/35436508>, 2022a.
- 501 He, X., X. Zheng, S. Zhang, X. Wang, T. Chen, X. Zhang, G. Huang, Y. Cao, L. He, X. Cao, Y. Cheng,
502 S. Wang & Y. Wu Comprehensive characterization of particulate intermediate-volatility and semi-
503 volatile organic compounds (I/SVOCs) from heavy-duty diesel vehicles using two-dimensional gas
504 chromatography time-of-flight mass spectrometry. *Atmos. Chem. Phys.*, 22, 13935-13947,
505 <https://dx.doi.org/10.5194/acp-22-13935-2022>, 2022b.
- 506 Huang, X. F., B. B. Zou, L. Y. He, M. Hu, A. S. H. Prévôt & Y. H. Zhang Exploration of PM_{2.5} sources
507 on the regional scale in the Pearl River Delta based on ME-2 modeling. *Atmos. Chem. Phys.*, 18, 11563-
508 11580, <https://acp.copernicus.org/articles/18/11563/2018/>, 2018.
- 509 Huo, Y., Z. Guo, Q. Li, D. Wu, X. Ding, A. Liu, D. Huang, G. Qiu, M. Wu, Z. Zhao, H. Sun, W. Song,
510 X. Li, Y. Chen, T. Wu & J. Chen Chemical Fingerprinting of HULIS in Particulate Matters Emitted from
511 Residential Coal and Biomass Combustion. *Environ Sci Technol*, 55, 3593-3603,
512 <https://www.ncbi.nlm.nih.gov/pubmed/33656861>, 2021.



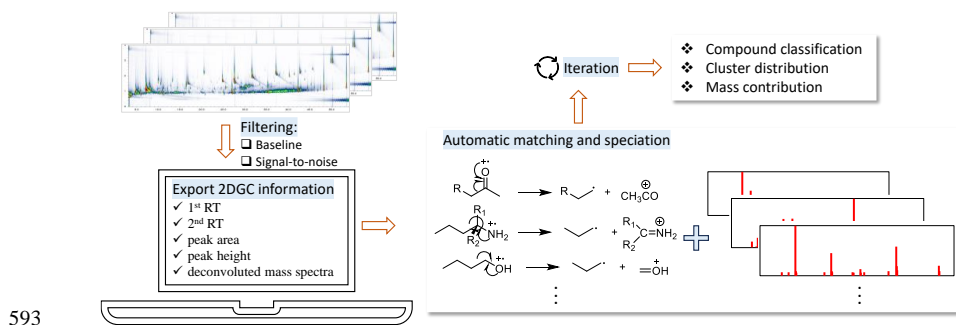
- 513 Kosyakov, D. S., N. V. Ul'yanovskii, T. B. Latkin, S. A. Pokryshkin, V. R. Berzhonskis, O. V. Polyakova
514 & A. T. Lebedev Peat burning - An important source of pyridines in the earth atmosphere. *Environ Pollut*,
515 266, 115109, <https://www.ncbi.nlm.nih.gov/pubmed/32622216>, 2020.
- 516 Kruve, A., K. Kaupmees, J. Liigand & I. Leito Negative electrospray ionization via deprotonation:
517 predicting the ionization efficiency. *Anal Chem*, 86, 4822-30,
518 <https://www.ncbi.nlm.nih.gov/pubmed/24731109>, 2014.
- 519 Phillips, K. A., A. Yau, K. A. Favela, K. K. Isaacs, A. McEachran, C. Grulke, A. M. Richard, A. J.
520 Williams, J. R. Sobus, R. S. Thomas & J. F. Wambaugh Suspect Screening Analysis of Chemicals in
521 Consumer Products. *Environ Sci Technol*, 52, 3125-3135,
522 <https://www.ncbi.nlm.nih.gov/pubmed/29405058>, 2018.
- 523 Piotrowski, P. K., B. A. Weggler, D. A. Yoxtheimer, C. N. Kelly, E. Barth-Naftilan, J. E. Saiers & F. L.
524 Dorman Elucidating Environmental Fingerprinting Mechanisms of Unconventional Gas Development
525 through Hydrocarbon Analysis. *Anal Chem*, 90, 5466-5473,
526 <https://www.ncbi.nlm.nih.gov/pubmed/29580048>, 2018.
- 527 Saeki, K., K. Ikari, H. Yokoi, S. I. Ohira, H. Okochi & K. Toda Biogenic Diamines and Their Amide
528 Derivatives Are Present in the Forest Atmosphere and May Play a Role in Particle Formation. *ACS Earth
529 and Space Chemistry*, 6, 421-430, 2022.
- 530 Shen, X., H. Che, Z. Yao, B. Wu, T. Lv, W. Yu, X. Cao, X. Hao, X. Li, H. Zhang & X. Yao Real-World
531 Emission Characteristics of Full-Volatility Organics Originating from Nonroad Agricultural Machinery
532 during Agricultural Activities. *Environ Sci Technol*, 57, 10308-10318,
533 <https://www.ncbi.nlm.nih.gov/pubmed/37419883>, 2023.
- 534 Silva, L. F. M., A. R. H. De La Cruz, A. H. M. Nunes & A. Gioda Real-Time Monitoring of Nitrogen
535 Oxides Emission Factors Using Sensors in the Exhaust Pipes of Heavy Vehicles in the Metropolitan
536 Region of Rio de Janeiro. *Journal of the Brazilian Chemical Society*, 2023.
- 537 Song, K., R. Tang, J. Zhang, Z. Wan, Y. Zhang, K. Hu, Y. Gong, D. Lv, S. Lu, Y. Tan, R. Zhang, A. Li,
538 S. Yan, S. Yan, B. Fan, W. Zhu, C. K. Chan & S. Guo. 2023. Molecular fingerprints and health risks of
539 home-use incense burning smoke. Copernicus GmbH.
- 540 Stanimirova, I., D. Q. Rich, A. G. Russell & P. K. Hopke A long-term, dispersion normalized PMF
541 source apportionment of PM_{2.5} in Atlanta from 2005 to 2019. *Atmospheric Environment*, 312, 120027,
542 2023.
- 543 Stefanuto, P.-H., A. Smolinska & J.-F. Focant Advanced chemometric and data handling tools for
544 GC×GC-TOF-MS Application of chemometrics and related advanced data handling in chemical
545 separations. *TrAC Trends in Analytical Chemistry*, 139, 116251, 2021.
- 546 Stout, S. A. & G. S. Douglas Diamondoid hydrocarbons - Application in the chemical fingerprinting of
547 natural gas condensate and gasoline. *Environmental Forensics*, 5, 225-235, 2004.
- 548 Wang, A. Q., Z. B. Yuan, X. H. Liu, M. L. Wang, J. Yang, Q. E. Sha & J. Y. Zheng Measurement-based
549 intermediate volatility organic compound emission inventory from on-road vehicle exhaust in China.
550 *Environmental Pollution*, 310, 2022.
- 551 Wang, G. L., S. B. Shi, P. R. Wang & T. G. Wang Analysis of diamondoids in crude oils using
552 comprehensive two-dimensional gas chromatography/time-of-flight mass spectrometry. *Fuel*, 107, 706-
553 714, 2013.
- 554 Wang, H., S. J. Zhang, X. M. Wu, Y. F. Wen, Z. H. Li & Y. Wu Emission Measurements on a Large
555 Sample of Heavy-Duty Diesel Trucks in China by Using Mobile Plume Chasing. *Environ Sci Technol*,
556 57, 15153-15161, 2023.



- 557 Welthagen, W., J. Schnelle-Kreis & R. Zimmermann Search criteria and rules for comprehensive two-
558 dimensional gas chromatography-time-of-flight mass spectrometry analysis of airborne particulate
559 matter. *J Chromatogr A*, 1019, 233-49, <https://www.ncbi.nlm.nih.gov/pubmed/14650618>, 2003.
- 560 Wong, Y. K., X. H. H. Huang, Y. Y. Cheng & J. Z. Yu Estimating primary vehicular emission
561 contributions to PM_{2.5} using the Chemical Mass Balance model: Accounting for gas-particle partitioning
562 of organic aerosols and oxidation degradation of hopanes. *Environmental Pollution*, 291, 118131, 2021.
- 563 Wu, L. L. & A. S. Geng Differences in the thermal evolution of hopanes and steranes in free and bound
564 fractions. *Organic Geochemistry*, 101, 38-48, 2016.
- 565 Xu, B., G. Zhang, O. Gustafsson, K. Kawamura, J. Li, A. Andersson, S. Bikkina, B. Kunwar, A. Pokhrel,
566 G. Zhong, S. Zhao, J. Li, C. Huang, Z. Cheng, S. Zhu, P. Peng & G. Sheng Large contribution of fossil-
567 derived components to aqueous secondary organic aerosols in China. *Nat Commun*, 13, 5115,
568 <https://www.ncbi.nlm.nih.gov/pubmed/36045131>, 2022.
- 569 Yan, J. Z., G. Wang, S. Y. Chen, H. Zhang, J. Q. Qian & Y. X. Mao Harnessing freight platforms to
570 promote the penetration of long-haul heavy-duty hydrogen fuel-cell trucks. *Energy*, 254, 124225, 2022.
- 571 Yu, D., Z. Tan, K. Lu, X. Ma, X. Li, S. Chen, B. Zhu, L. Lin, Y. Li, P. Qiu, X. Yang, Y. Liu, H. Wang,
572 L. He, X. Huang & Y. Zhang An explicit study of local ozone budget and NO_x-VOCs sensitivity in
573 Shenzhen China. *Atmospheric Environment*, 224, 117304,
574 <https://www.sciencedirect.com/science/article/pii/S1352231020300467>, 2020.
- 575 Zang, W., R. Sharma, M. W. Li & X. Fan Retention Time Trajectory Matching for Peak Identification
576 in Chromatographic Analysis. *Sensors (Basel)*, 23, 6029,
577 <https://www.ncbi.nlm.nih.gov/pubmed/37447878>, 2023.
- 578 Zhang, Y., R. Li, J. Fang, C. Wang & Z. Cai Simultaneous determination of eighteen nitro-polyaromatic
579 hydrocarbons in PM_{2.5} by atmospheric pressure gas chromatography-tandem mass spectrometry.
580 *Chemosphere*, 198, 303-310, <https://www.ncbi.nlm.nih.gov/pubmed/29421744>, 2018.
- 581 Zhao, Y., C. J. Hennigan, A. A. May, D. S. Tkacik, J. A. de Gouw, J. B. Gilman, W. C. Kuster, A. Borbon
582 & A. L. Robinson Intermediate-volatility organic compounds: a large source of secondary organic
583 aerosol. *Environ Sci Technol*, 48, 13743-137550, <https://www.ncbi.nlm.nih.gov/pubmed/25375804>,
584 2014.
- 585 Zhao, Y., N. T. Nguyen, A. A. Presto, C. J. Hennigan, A. A. May & A. L. Robinson Intermediate
586 Volatility Organic Compound Emissions from On-Road Diesel Vehicles: Chemical Composition,
587 Emission Factors, and Estimated Secondary Organic Aerosol Production. *Environ Sci Technol*, 49,
588 11516-11526, <https://www.ncbi.nlm.nih.gov/pubmed/26322746>, 2015.
- 589 Zhao, Y., D. S. Tkacik, A. A. May, N. M. Donahue & A. L. Robinson Mobile Sources Are Still an
590 Important Source of Secondary Organic Aerosol and Fine Particulate Matter in the Los Angeles Region.
591 *Environ Sci Technol*, 56, 15328-15336, <https://www.ncbi.nlm.nih.gov/pubmed/36215417>, 2022.



592 For Table of Contents Only



593